nature COMMUNICATIONS

ARTICLE

Received 10 Apr 2013 | Accepted 23 Aug 2013 | Published 20 Sep 2013

DOI: 10.1038/ncomms3499 OPEN

Strongly enhanced flux pinning in one-step deposition of $BaFe_2(As_{0.66}P_{0.33})_2$ superconductor films with uniformly dispersed $BaZrO_3$ nanoparticles

Masashi Miura[1,2], Boris Maiorov[3], Takeharu Kato[4], Takashi Shimode[1], Keisuke Wada[1], Seiji Adachi[1] & Keiichi Tanabe[1]

The high upper critical field and low anisotropy of the iron-based superconductor $BaFe_2As_2$ make it promising for its use in the construction of superconducting magnets. However, its critical current density in high magnetic fields needs to be improved. Here we demonstrate a simple, one-step and industrially scalable means of achieving just this. We show that introducing controlled amounts of uniformly dispersed $BaZrO_3$ nanoparticles into carrier-doped $BaFe_2As_2$ significantly improves its superconducting performance without degrading its structural or superconducting properties. Our $BaFe_2(As_{0.66}P_{0.33})_2$ films also exhibit an increase in both the irreversibility line and critical current density at all magnetic-field orientations. These films exhibit nearly isotropic critical current densities in excess of 1.5 MA cm^{-2} at 15 K and 1 T—seven times higher than previously reported for $BaFe_2As_2$ films. The vortex-pinning force in these films reaches $\sim$59 GN m^{-3} at 5 K and 3–9 T, substantially higher than that of the conventional Nb_3Sn wire.

[1] Superconductivity Research Laboratory, International Superconductivity Technology Center, 10-13, Shinonome 1-chome, Koto-ku, Tokyo 135-0062, Japan. [2] Graduate School of Science and Technology, Seikei University, 3-3-1 Kichijoji-kitamachi, Musashino-shi, Tokyo 180-8633, Japan. [3] Division of Materials Physics and Applications, Los Alamos National Laboratory, Los Alamos, New Mexico 87545, USA. [4] Materials R&D Laboratory, Japan Fine Ceramics Center, 2-4-1 Mutsuno, Atuta-ku, Nagoya 456-8587, Japan. Correspondence and requests for materials should be addressed to M.M. (email: masashi-m@st.seikei.ac.jp).

In the search for new classes of superconductors that might replace NbTi and $NbSn_3$, the new iron-based superconductors, in particular carrier-doped $BaFe_2As_2$ (Ba122), have attracted much attention, as they exhibit high upper critical field[1] and low anisotropy[2]. The powder-in-tube technology has been progressing well for K-doped Ba122 (Ba122:K) and Co-doped Ba122 (Ba122:Co) wires[3,4]. However, their critical current density (J_c) values in a magnetic field are still low, thus indicating the need for flux pinning improvement.

As an alternative technology, some groups have indicated the potential of biaxially textured thin-film processing for Ba122:Co-coated conductors[5,6]. Although these Ba122:Co films show relatively high J_c at self-field ($J_c^{s.f.}$) of over 1 MA cm^{-2} at 4.2 K (because of low misorientation angles at grain boundaries), J_c decays rather rapidly when a magnetic field is applied. The decrease in J_c in a magnetic field depends on the ability of pinning flux lines, which is determined by the defects that have to be tailored into the material without degrading the current pathway. Indeed, flux pinning has been also one of the most important topics in high-temperature superconductors, such as $REBa_2Cu_3O_y$(RE = rare-earth elements; RE123) for electric-power applications[7–13]. Following the well-known technique of heavy ion irradiation[14], recently, amorphous tracks induced by heavy-ion irradiation in Ba122:K single crystals[15] were shown to enhance J_c at high fields. This irradiation resulted in a matching field as high as 21 T, with no critical temperature (T_c) degradation. Although heavy-ion irradiation is not practical for long-length wire and tape applications, this work shows that Ba122:K can tolerate a very high density of defects without significant crystalline degradation. However, films of Ba122:K are unlikely to be made *in situ* because of the high vapour pressure of K. On the other hand, irradiation with protons and heavy ions in Ba122:Co showed clear negative effects in terms of T_c degradation[16–18]. Several Ba122:Co films showed strong *c* axis pinning because of naturally introduced nanopillars, or defects, which can increase J_c around the *c* axis direction[19–21], without a big improvement around the *ab*-plane orientation. The naturally occurring defects are difficult to control, indicating the need of a controllable, tunable and practical way to increase vortex pinning in Ba122 films in an isotropic way. Following the outstanding achievements for cuprates[7–13], the addition of second phases is a potentially useful technique here. However, in iron-based pnictides, FeAs is known to have a great tendency to segregate at grain boundaries, thus becoming a blocking phase[22]. In order to contribute to the current transport, the second phase needs to be chemically stable and crystallographically compatible, and its size should be sufficiently small to avoid blocking of the current path.

Here we report a new one-step strategy that leads to an oxide second phase, resulting in a strong vortex pinning landscape for P-doped Ba122 superconductor films. This is developed on the basis of the easily scalable pulsed laser deposition (PLD) technique. The artificial vortex pinning centres originate from a very dense array of $BaZrO_3$ (BZO) nanoparticles randomly dispersed within $BaFe_2(As_{0.66}P_{0.33})_2$ (Ba122:P) films with virtually no degradation of T_c. We chose Ba122:P because it has a T_c of ~30 K[23], higher than that of Ba122:Co[5,6], and is chemically more stable than Ba122:K[24]. Angle-dependent $J_c(H,T)$ measurements demonstrate that the new strategy is highly effective in preventing vortex motion at high fields, at both 5 and 15 K and for all magnetic-field orientations. A remarkably high pinning force, well over the values for low-temperature superconductors at 4.2 K, is also achieved at both 5 and 15 K.

Results

Uniformly dispersed $BaZrO_3$ in $BaFe_2(As_{0.66}P_{0.33})_2$ films. Epitaxial BZO-doped Ba122:P (Ba122:P + BZO) thin films (thickness ~80 nm) were grown from 1 mol.% and 3 mol.% BZO-doped PLD targets, and their microstructure was studied by different techniques (see Methods). Spectral maps of Fe, As, Zr, Ba and P for a Ba122:P + 3 mol.%BZO film are shown in Fig. 1a–e, respectively, with Fig. 1f showing a cross-sectional transmission electron microscopy (TEM) image. From these images, the presence of uniformly dispersed nanoparticles can be observed. These particles are rich in Zr and poor in Fe, As and P. Ba appears to be homogenously distributed through the film's thickness; this and the Zr-rich zones suggest the presence of a Ba-Zr-containing phase. The spectral maps yield an average nanoparticle size of ~8 nm with an average spacing L ~24 nm, leading to a density $n \sim 6.8 \times 10^{22}$ m^{-3}. XRD patterns in Fig. 2a indicate that the doped film shows a peak consistent with the $BaZrO_3$ (110) peak, also consistent with the spectral image of Zr and Ba. As the (200) peak of BZO almost overlaps the (200) peak of the MgO single crystal substrate, it was not possible to conclude about epitaxial film orientation. Figure 2b shows a cross-sectional high-resolution TEM image of the Ba122:P + 3 mol.%BZO film, where the electron beam is along <010> of the

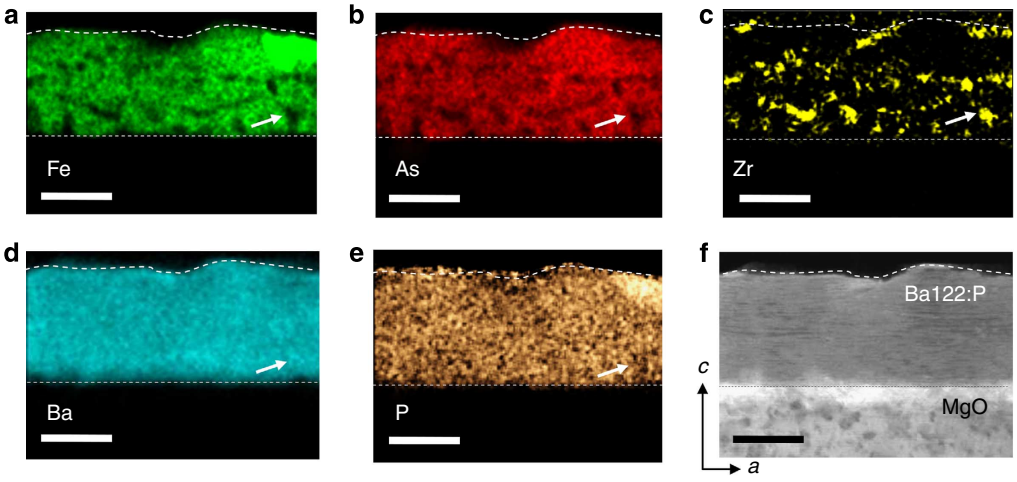

Figure 1 | Cross-sectional elemental maps of a Ba122:P + BZO film. Elemental maps of the Ba122:P + 3 mol. %BZO film for Fe, As, Zr, Ba and P, (**a**–**e**), respectively. (**f**) Cross-sectional low-magnification TEM image. The arrows in (**a**–**e**) indicate dispersed Ba-Zr-containing nanoparticles. Each horizontal bar indicates 50 nm scale.

Ba122:P matrix. A BZO nanoparticle can be clearly discerned within the matrix, its size being ~5 and ~10 nm parallel and perpendicular to the *c* axis, respectively (vertical arrow). Moreover, a slight strain is observed in the *ab*-plane around the nanoparticle, similar to what is observed in some RE123 films with nanoparticles[25]. In turn, the periodicity of Ba122 planes around the BZO nanoparticle is only perturbed by the creation of stacking faults (horizontal arrows). Further identification of these nanoparticles is achieved using nano-beam diffraction (Fig. 2c,d). Diffraction patterns of the Ba122:P matrix shown in Fig. 2c indicate that the Ba122:P matrix is epitaxially oriented on the MgO substrate. On the other hand, for the BZO nanoparticle (see Fig. 2d), we confirm a diffraction spot of the [110] for BZO—that is, the <110> of BZO is tilted from the <010> of the Ba122:P matrix; the BZO nanoparticles are not epitaxially oriented along the Ba122:P matrix.

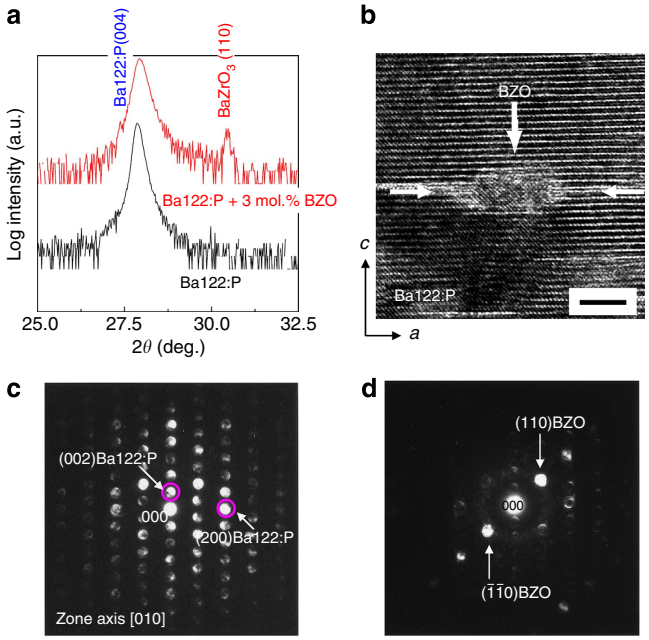

Figure 2 | Microstructural characterization of a Ba122:P + BZO film. (**a**) Out-of-plane θ-2θ, X-ray diffraction patterns of Ba122:P and Ba122:P + 3mol.%BZO films. The $BaZrO_3$ phase is identified in only film with BZO. (**b**) Cross-sectional high-resolution TEM image of the Ba122:P + 3mol.%BZO film, in which a BZO nanoparticle with the height and diameter of ~ 5 and ~ 10 nm, respectively (vertical arrow) can be easily discerned within the matrix. The horizontal arrows point to stacking faults observed around the nanoparticle. The horizontal bar scale indicates 5 nm for (**b**). (**c**) Diffraction pattern of the Ba122:P matrix showing that the matrix is coherent with the MgO substrate. (**d**) Nano-beam diffraction pattern of the BZO nanoparticle showing that it is not coherent with the Ba122:P matrix.

Table 1 shows a summary of crystallographic and superconducting properties for the Ba122:P and several Ba122:P films with BZO. The superconducting transition temperature ($T_{c,zero}$) of the films was determined by means of electrical transport measurements and is ~26 K for the Ba122:P film, whereas a slightly lower T_c (~1 K lower) is observed for the films where BZO was added. This decrease is independent of the BZO percentage added and does not affect the crystalline quality of the matrix as seen in Table 1. Even though the Ba122:P + BZO films have slightly lower T_cs, the $J_c^{s.f.}$s are significantly higher. The $J_c^{s.f.}$ of Ba122:P + 3 mol.%BZO films at 5 and 15 K are >5 and 3 MA cm^{-2}, respectively. These $J_c^{s.f.}$ values are almost as high as those of Ba122:K single crystals irradiated with a dose of $B_\phi = 21$ T[15] and higher than those of Ba122:Co films[17].

Upper critical field and improved irreversibility field. Figure 3a shows the normalized temperature ($t = T/T_c$) dependence of the upper critical field, H_{c2} for **H**||*c* and **H**||*ab* for the Ba122:P and Ba122:P + 3 mol.%BZO films. H_{c2} is remarkably similar for both films in spite of their very different pinning landscapes, as is also observed in cuprate superconductors where the coherence length is very small. We extracted the superconducting mass anisotropy (γ_H) using anisotropic scaling[26] and found that the films with and without BZO can be described well with $\gamma_H \sim 1.50$, which is slightly smaller than γ_H for Ba122:Co and Sr122:Co films at the same temperatures[21,27,28]. These values are in good agreement with the $\gamma \sim 1.55$ value extracted from the angular dependence of H_{c2} ($t = 0.90$) for the Ba122:P film and the Ba122:P + 3 mol.%BZO film (see inset of Fig. 3a).

The Ba122 films show a small but sizable vortex liquid region between H_{c2} and the irreversibility field H_{irr}, where $J_c = 0$. Reducing the vortex liquid region is of great interest, as it expands the 'useful' vortex phase diagram. In Fig. 3b, we show the H_{irr}–t diagram at **H**||*c* and **H**||*ab*. Although H_{irr} increases slightly after the BZO addition for **H**||*ab*, H_{irr} shows a striking increase for **H**||*c*. The increase is such that H_{irr}(Ba122:P + 3 mol.%BZO) at low fields parallel to the *c* axis is as high as for **H**||*ab* and higher than H_{irr}(Ba122:P) for any orientation. The improvement is maximized around $\mu_0 H \sim 3$ T, where the intervortex distance is $a_f \sim 28$ nm, which is close to the average distance between BZO nanoparticles ($L \sim 24$ nm) observed in TEM. This suggests that the maximum reduction in the vortex liquid region occurs when the intervortex spacing corresponds to the distance between nanoparticles. The drastic shrinkage in the vortex liquid phase is very promising and is much more beneficial than that observed in cuprates.

Dramatically high J_c with nearly isotropic angular dependence. In Fig. 4a, we show the field dependence of J_c(**H**||*c*) at 5 K for the reference and BZO-added Ba122:P films. We highlight two major results here; one, that the $J_c^{s.f.}$ increases monotonically with the amount of BZO additive (also see Table 1) and that the field decay of J_c is greatly reduced within the measured field range, indicating a massive improvement in vortex pinning. Further

Table 1 | Structural and superconducting properties.

Material	$\delta\omega$ (deg.)	$\delta\phi$ (deg.)	$T_{c,zero}$ (K)	$J_c^{s.f.}$ at 5 K (MA cm^{-2})	$J_c^{s.f.}$ at 15 K (MA cm^{-2})
Ba122:P	0.75	1.03	26.3	3.0	1.4
Ba122:P + 1mol.% BZO	0.8	1.05	25.3	3.7	2.2
Ba122:P + 3 mol.% BZO (A)	0.79	1.06	25.0	5.2	3.0
Ba122:P + 3 mol.% BZO (B)	0.81	1.09	25.1	5.0	2.9

Sample data for the reference Ba122:P film and for Ba122:P + $BaZrO_3$ films on single crystal MgO. $T_{c,zero}$ was determined using an 0.01ρ_n criterion. $\delta\omega$ and $\delta\phi$ denote the full-width at half-maximum (FWHM) values of out-of-plane rocking curves (ω scans) of the 004 diffractions and in-plane rocking curves (ϕ scans) of the 103 diffractions, respectively. Two Ba122:P + 3mol.%BZO films (A and B) show almost identical properties.

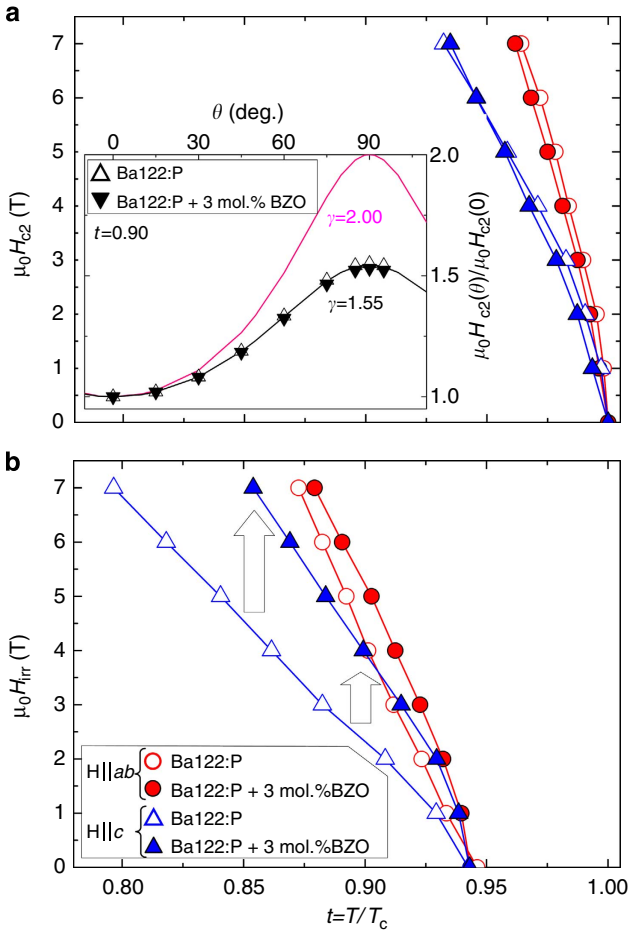

Figure 3 | Upper critical field $H_{c2}(T)$ and irreversibility field $H_{irr}(T)$. (**a**) Normalized temperature ($t=T/T_c$) dependence of H_{c2} for Ba122:P and Ba122:P + 3mol.%BZO films at **H**||*c* and **H**||*ab*. Inset: angular dependence of H_{c2} at $t=0.90$ for Ba122:P and Ba122:P + 3mol.%BZO films follow a curve consistent with $\gamma \sim 1.55$. (**b**) Normalized temperature dependence of H_{irr} at **H**||*c* and **H**||*ab*.

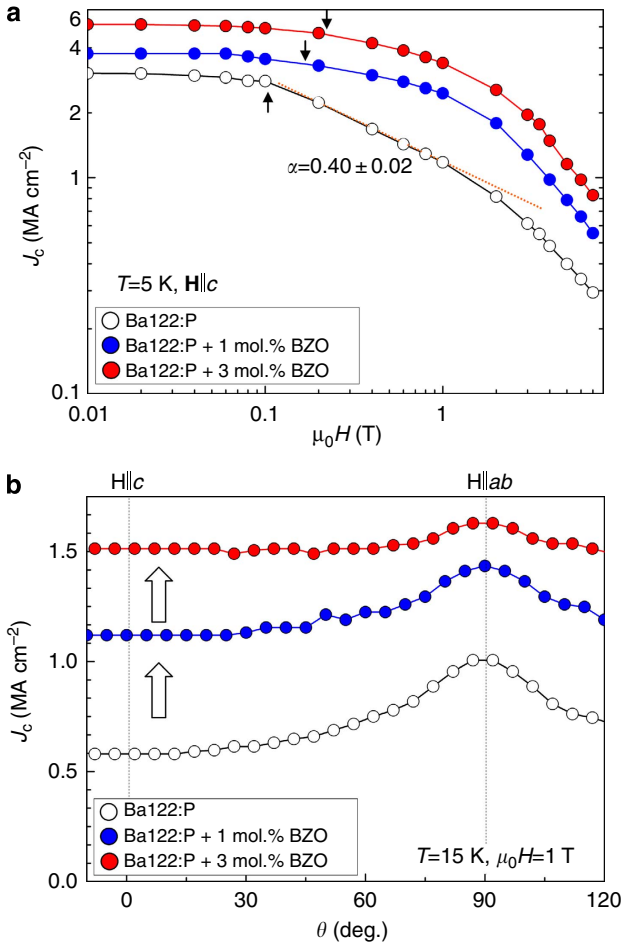

Figure 4 | Critical current density as a function of magnetic field and angle. (**a**) J_c(**H**||*c*) at 5 K for Ba122:P + 1mol.%BZO and Ba122:P + 3mol.%BZO films compared with the Ba122:P film. The arrows indicate the positions of the crossover field H^*. (**b**) Angular dependence of J_c at 15 K, 1 T for Ba122:P and Ba122:P films with BZO.

analysis allows us to find the key indicators pointing to the area and reasons for improvement. For Ba122:P films, we observe at low fields that J_c is nearly constant up to a characteristic crossover field H^* (90% of $J_c(H)/J_c^{s.f.}$), followed by a power-law regime ($J_c \propto H^{-\alpha}$) at intermediate fields. Finally, at yet higher fields a more rapid decay of J_c is observed as H approaches H_{irr}. For the Ba122:P film, we find $\alpha \sim 0.40$ at both 5 and 15 K, which is close to but slightly smaller than the values observed in typical RE123 films with weak point-like defects[29].

We now turn our attention to the Ba122:P + BZO films. Besides the increase in $J_c^{s.f.}$, H^* also increases with BZO content (see arrows in Fig. 4a). This increase in H^* for films with BZO nanoparticles is consistent with the typical effect of nanoparticles[30,31], as the low-field regime is determined to be the single vortex pinning regime. At intermediate fields, we find that both films with BZO show a slower decay of $J_c(H)$, indicative of the importance of BZO nanoparticles to enhance $J_c(H)$ in a magnetic field. This improvement in $J_c(H)$ is manifested such that $J_c(H)$ does not follow a power-law dependence as in the Ba122:P standard film. This type of non-power-law dependence is similar to that observed in RE123 films, with strong pinning coming from uniformly dispersed nanoparticles[11,12,32,33].

Further insight into the effects of the BZO addition to the pinning landscape of the Ba122:P films can be obtained from the angular-dependent J_c. Figure 4b shows $J_c(\theta)$ curves measured for the three films at 1 T, 15 K. Upon addition of BZO, J_c increases for all orientations with respect to the J_c of the Ba122:P film. Similar to $J_c^{s.f.}$, the improvement is cumulative with increasing BZO content; the increase in J_c for the Ba122:P + 3 mol.%BZO film is 2.6 times higher than that of the Ba122:P film. It is worth noting that for our Ba122:P + 3 mol.%BZO film, we achieve a $J_{c,min}$ of 1.5 MA cm^{-2} at 1 T, 15 K, which is over 28 times and 7 times higher than that of Ba122:Co films with *c* axis columnar defects[19] and Ba122:Co films with superlattice structures[34], respectively, in very similar field and temperature conditions. Moreover, the J_c value of the Ba122:P + 3 mol.%BZO film is almost the same as that of proton-irradiated Ba122:Co films at 1 T, despite the former being over 10 K higher in temperature[17].

The remarkable in-field performance of Ba122:P films with BZO is highlighted in Fig. 5, where the pinning force, $F_p = J_c(H) \times \mu_0 H$ is compared with that of several superconductor materials. At 15 K, F_p is over three times higher for the Ba122:P + 3 mol.%BZO film than for the Ba122:P film and higher than NbTi[35] at 4.2 K at all magnetic fields; we also find that F_p is clearly higher for $\mu_0 H > 0.5$ T when compared with MgB_2 data at 15 K[36]. At $T=5$ K, the F_p of the Ba122:P + 3 mol.%BZO film reaches ~ 59 GN m^{-3} for $\mu_0 H > 3$ T up to the highest field we measured (9 T)—a 50% increase over Nb_3Sn at 4.2 K[37]. This F_p

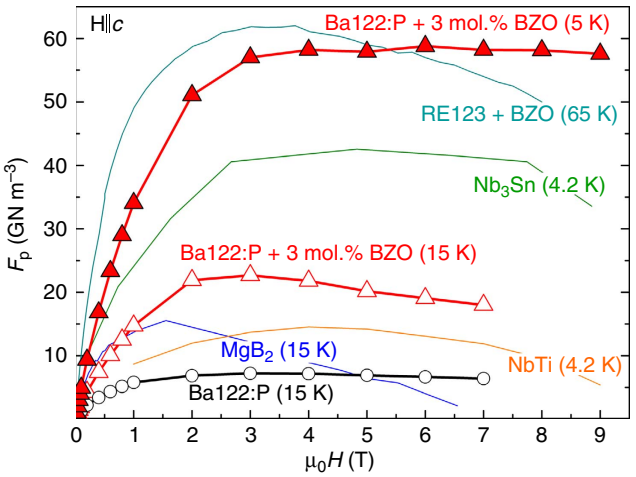

Figure 5 | Pinning force F_p for various superconducting materials. The F_p-$\mu_0 H$ curves of Ba122:P + 3mol.%BZO film at 5 and 15 K and the Ba122 film at 15 K. For comparison, the data for NbTi[35] at 4.2 K, MgB_2(H||*ab*)[36] at 15 K, Nb_3Sn[37] at 4.2 K and RE123 + BZO-coated conductor[38] at 65 K are included.

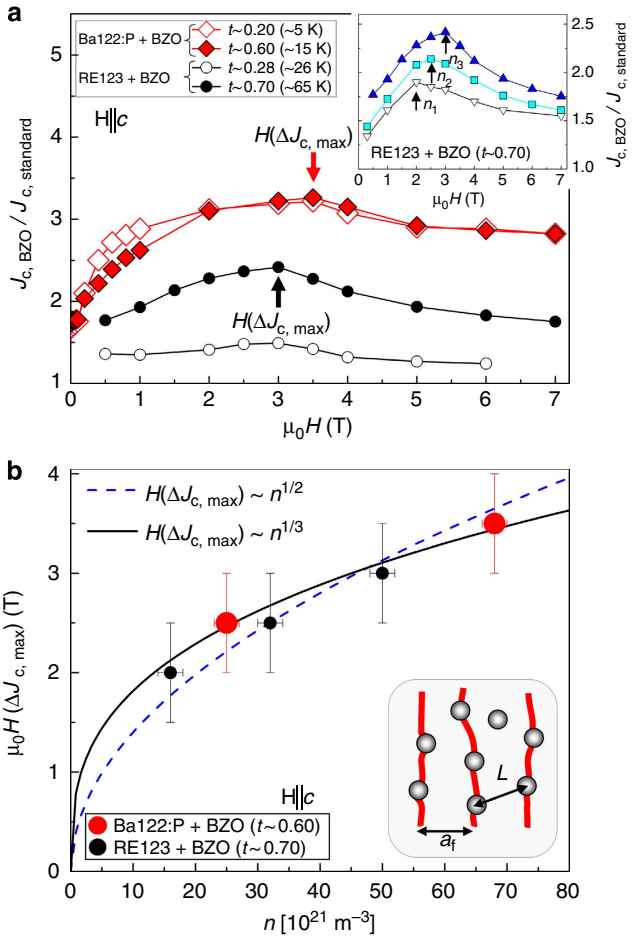

Figure 6 | Field and nanoparticle-density behaviour of the J_c ratio. (**a**) The J_c ratio ($\Delta J_c = J_{c,BZO}/J_{c,standard}$) at **H**||*c* for Ba122:P films at $t \sim 0.2$ and $t \sim 0.6$. For comparison, the data for RE123 films at $t \sim 0.28$ and $t \sim 0.70$ are included. Inset: $J_{c,BZO}/J_{c,standard}$ at $t \sim 0.70$ and **H**||*c* for RE123 with different BZO nanoparticle densities ($n_1 = 1.6 \times 10^{22}$, $n_2 = 3.1 \times 10^{22}$ and $n_3 = 5.0 \times 10^{22}\,m^{-3}$). (**b**) Solid symbols, $H(\Delta J_{c,max})$ at **H**||*c* for Ba122:P films at $t \sim 0.60$; open symbols, $H(\Delta J_{c,max})$ at **H**||*c* for RE123 films at $t \sim 0.70$. Inset: Schematic of a possible configuration of each vortex line is pinned by an array of nanoparticles. Vertical error bars were determined by the magnetic field-measuring intervals; horizontal ones represent the dispersion of the density value obtained from different TEM images.

value is comparable to that of the RE123-coated conductor with BZO nanoparticles at 65 K[38]. Please note that because the pinning landscape is produced by nanoparticles (and not *c* axis-oriented nanorods), F_p measured along the *c* axis is just the minimum value for a given field.

Simple analysis tool of vortex pinning by nanoparticles. One important aspect of engineering a pinning landscape is the ability of tuning it for maximizing the performance at a particular desired field. One way to characterize the effect of a given pinning improvement route is to calculate the J_c enhancement ratio. This of course needs to be performed starting with a state of the art reference sample, the 'standard'. In Fig. 6a, we present the field dependence of the ratio $J_{c,BZO}/J_{c,standard}$ for Ba122:P films at $t = T/T_c = 0.20$ and $t = 0.60$. As for the validity/universality of this approach, we also plot the ratio for RE123 films with a similar density of BZO nanoparticles at the same fields and very similar *t*. We observe that the J_c ratios for the Ba122:P films at both temperatures are very similar, with a maximum around $\mu_0 H(\Delta J_{c,max}) \sim 3.5$ T ($H(\Delta J_{c,max})$ is the field value at the maximum $\Delta J_c = J_{c,BZO}/J_{c,standard}$). For the case of RE123, the J_c ratio exhibits a significant enhancement at $\mu_0 H(\Delta J_{c,max}) \sim 3.0$ T at high temperatures only, and no clear improvement is found at low temperatures. The similarity of the ratio increase between RE123 at $t = 0.70$ and Ba122:P is remarkable, both in the peak position and amplitude. This result also points out that the BZO inclusions seem to be more effective in Ba122 than in RE123 and in a wider temperature range.

This difference in effectiveness stems from the nanoparticle size relative to the vortex core size at different temperatures. The BZO nanoparticles in the Ba122:P films are $d \sim 8$ nm in diameter, which is a good size to pin a vortex core given its size at either 5 K ($2\xi_{ab} \sim 5$ nm, $d/2\xi_{ab} = 1.6$) or 15 K ($2\xi_{ab} \sim 8$ nm, $d/2\xi_{ab} = 1.0$). The BZO nanoparticles in RE123 films are bigger with diameter $d \sim 25$ nm. Thus, $d/2\xi_{ab} = 3.1$ ($2\xi_{ab} \sim 8.1$ nm) at 65 K, which is still effective but not as much as in Ba122:P films. At low temperatures, the size of these particles in RE123 films is much larger than the vortex cores with $d/2\xi_{ab} = 5.0$ ($2\xi_{ab}(26\,K) \sim 5.0$ nm), resulting in no significant pinning enhancement even at densities as high as $n = 5.0 \times 10^{22}\,m^{-3}$. These results lead us to deduce that the maximum nanoparticle size for effective pinning needs to be no larger than $d/2\xi_{ab}(T) \cong 3$.

As mentioned above, $H(\Delta J_{c,max})$ is temperature-independent for Ba122:P with BZO and has a value very close to that found for RE123 at high *t*, for a film with a similar BZO nanoparticle density. Indeed, the intervortex distances for $\mu_0 H(\Delta J_{c,max}) = 3.5$ and 3.0 T (see Fig. 6a) are 26 and 28 nm, respectively, which are very close to the interparticle spacing determined using TEM of ~24 and ~27 nm, respectively. Furthermore, this correlation is reinforced by the results shown in the inset of Fig. 6a, where a clear increase in $H(\Delta J_{c,max})$ is observed with increasing density of BZO nanoparticles for RE123 films. These results indicate that $H(\Delta J_{c,max})$ increases monotonically with increasing particle density.

This is further reflected in Fig. 6b, where $H(\Delta J_{c,max})$ is plotted against *n* for Ba122:P ($t \sim 0.60$) and RE123 ($t \sim 0.70$) films. A clear universal dependence of $H(\Delta J_{c,max})$ on *n* is observed for both types of films. This dependence can be fitted with a power law, such that $H(\Delta J_{c,max}) \sim n^{1/3 \sim 1/2}$. The latter dependence is

consistent with the observation that $a_f \sim L$. This is shown schematically in the inset of Fig. 6b, in which the vortex line separation is the same as the distance between nanoparticles. This indicates that the maximum improvement in J_c produced by the BZO nanoparticle additions occurs when the elastic energy (that is, vortex repulsive interactions) of the vortices is minimized to accommodate to the strong pinning exerted by the nanoparticles.

This phenomenological model is valid in the density range of technological interest and leads to $\mu_0 H(\Delta J_{c,max}) = 0$ for no added particles. Koshelev *et al.*[39] studied theoretically the effect of an array of nanoparticles on the vortex line pinning and found that the critical current is determined by the length of the trapped segment, leading to $L \propto n$. In this model, the critical force grows roughly as $n^{1/2}$. From the experimental results and the theoretical analysis above, we find a simple but effective rule for optimizing the performance of a material at a given magnetic field for both iron-pnictides and cuprates with nanoparticles. Namely, process the material to yield nanoparticles with average size smaller than $\sim 3 \times (2\xi(T))$ and with densities such that the nanoparticle spacing matches the intervortex distance at the given magnetic field $H(\Delta J_{c,max})$.

Discussion

For application to magnets, an isotropic field angular dependence of J_c is as important as its value. A significant increase in J_c around the *c* axis direction was reported for the Ba122:Co films with naturally introduced nanopillars (or defects)[19–21]. Although Ba122:Co films with superlattice structures were recently shown to have an improved J_c not only in the *c* axis but also in the *ab*-plane directions, the angular dependence of J_c is still anisotopic[34]. We achieved a notably high $J_{c,min}$ with nearly isotropic angular dependence (the ratio $J_{c,max}/J_{c,min} = 1.1$) by simply adding $BaZrO_3$ nanoparticles. The present achievement offers a method for developing novel superconducting tapes, and possibly cables, with a simple one-step deposition and industrially scalable production process that can be used to make high-field magnets for operation in the temperature range up to 15 K. At the same time, our simple analysis tool allows the application of this method to any superconductor for better tuning and engineering of the critical current improvements.

The drastic reduction in the extend of vortex liquid phase region and large isotropic critical current obtained indicate a fruitful route for improving other iron-pnictide materials. Rethinking the role of the superconducting matrix and its ability of withstanding large amounts of material defects and inclusions is also critical to increasing vortex pinning without blocking superconducting currents. Thus, an important effort should be concentrated in this area both in iron- and copper-based superconductors.

Methods

PLD target preparation for $BaFe_2(As_{0.66}P_{0.33})_2$ films. Polycrystalline PLD targets with the nominal compositions of $BaFe_2(As_{0.66}P_{0.33})_2$, $BaFe_2(As_{0.66}P_{0.33})_2 + 1$ mol.% $BaZrO_3$ and $BaFe_2(As_{0.66}P_{0.33})_2 + 3$ mol.% $BaZrO_3$ were sintered following standard procedures. As starting materials, Ba metal (99.99%, chunk), Fe metal (99.9%, no. 300 mesh pass), As powder (99.9999%, ~3 μm grain) and P powder (99.999%, no. 600 mesh pass) were used. Processing was carried out in an argon-filled glove box. Ba metal was cut into small pieces to promote reaction. Ba and As at a ratio of 1:1 were put into an alumina tube. It was sealed in an evacuated quartz tube and heat-treated at 500 °C for 10 h and 650 °C for 20 h. A similar procedure was carried out for $FeAs_{0.17}P_{0.33}$ in nominal composition. The reacted materials were pulverized using an agate mortar and mixed together in a ratio of $BaAs:FeAs_{0.17}P_{0.33} = 1:2$. The powder mixture was press-formed into a pellet, reacted at 650 °C for 10 h and 900 °C for 24 h in an evacuated quartz tube. Then, 1 and 3 mol% of $BaZrO_3$ powder (Toshima Manufacturing Co. Ltd) were added to the above $BaFe_2(As_{0.67}P_{0.33})_2$ powder, reacted at 1,000 °C for 24 h.

$BaFe_2(As_{0.66}P_{0.33})_2$ films with $BaZrO_3$ nanoparticles. Epitaxial films (~80 nm in thickness) were deposited on MgO (100) single crystal substrates by ablating the polycrystalline PLD targets using the second harmonic (wavelength: 532 nm) of a pulsed Nd:YAG laser at a repetition rate of 10 Hz in vacuum of 10^{-4} Pa at a substrate temperature of 800 °C. Film thickness was measured from cross-sectional TEM images at several points and ranged from 72 to 80 nm.

Transport properties in magnetic fields. Films were patterned using photolithography and ion milling into bridges of ~50 μm width. The crystalline quality was examined using XRD. The temperature dependence of the resistivity (ρ) was measured by a four-probe method in the temperature range of 10–300 K using a Quantum Design PPMS with a superconducting magnet generating a field **H** of up to 9 T. In the PPMS, a rotational stage was used to rotate the samples with respect to **H**. The H_{c2} and H_{irr} were determined using 0.90 ρ_N and 0.01ρ_N criteria, respectively, where ρ_N is the normal-state resistivity. The critical current was determined using a 1 μV cm^{-1} criterion.

Microstructure and chemical composition analysis. The microstructures and elemental concentration mappings of the films were analysed by TEM and energy-dispersive X-ray spectroscopy, respectively.

References

1. Tarantini, C. *et al.* Significant enhancement of upper critical fields by doping and strain in iron-based superconductors. *Phys. Rev. B* **84,** 184522 (2011).
2. Putti, M. *et al.* New Fe-based superconductors: properties relevant for applications. *Supercond. Sci. Tech.* **23,** 034003 (2010).
3. Weiss, J. D. *et al.* High intergrain critical current density in fine-grain $(Ba_{0.6}K_{0.4})Fe_2As_2$ wires and bulks. *Nat. Mater.* **11,** 682–685 (2012).
4. Ma, Y. *et al.* Progress in wire fabrication of iron-based superconductors. *Supercond. Sci. Tech.* **25,** 113001 (2012).
5. Katase, T. *et al.* Biaxially textured cobalt-doped $BaFe_2As_2$ films with high critical current density over 1 MA cm^{-2} on MgO-buffered metal-tape flexible substrates. *Appl. Phys. Lett.* **98,** 242510 (2011).
6. Iida, K. *et al.* Epitaxial growth of superconducting $Ba(Fe_{1-x}Co_x)_2As_2$ thin films on technical ion beam assisted deposition MgO substrates. *Appl. Phys. Express.* **4,** 013103 (2011).
7. Foltyn, S. R. *et al.* Materials science challenges for high-temperature superconducting wire. *Nat. Mater.* **6,** 631–642 (2007).
8. Larbalestier, D., Gurevich, A., Feldmann, D. M. & Polyanskii, A. High-T_c superconducting materials for electric power applications. *Nature* **414,** 368–377 (2001).
9. MacManus-Driscoll, J. L. *et al.* Strongly enhanced current densities in superconducting coated conductors of $YBa_2Cu_3O_{7-x} + BaZrO_3$. *Nat. Mater.* **3,** 439–443 (2004).
10. Haugan, T., Barnes, P. N., Wheeler, R., Meisenkothen, F. & Sumption, M. Addition of nanoparticle dispersions to enhance flux pinning of the $YBa_2Cu_3O_{7-x}$ superconductor. *Nature* **430,** 867–870 (2004).
11. Gutiérrez, J. *et al.* Strong isotropic flux pinning in $YBa_2Cu_3O_{7-x} + BaZrO_3$ films derived from chemical solutions. *Nat. Mater.* **6,** 367–373 (2007).
12. Maiorov, B. *et al.* Synergetic combination of different types of defect to optimize pinning landscape using $BaZrO_3$-doped $YBa_2Cu_3O_7$. *Nat. Mater.* **8,** 398–404 (2009).
13. Llordés, A. *et al.* Nanoscale strain-induced pair suppression as a vortex-pinning mechanism in high temperature superconductors. *Nat. Mater.* **11,** 329–336 (2012).
14. Civale, L. *et al.* Vortex confinement by columnar defects in $YBa_2Cu_3O_7$ crystals: enhanced pinning at high fields and temperatures. *Phys. Rev. Lett.* **67,** 648–651 (1991).
15. Fang, L. *et al.* High, magnetic field independent critical currents in $(Ba,K)Fe_2As_2$ crystals. *Appl. Phys. Lett.* **101,** 012601 (2012).
16. Tamegai, T. *et al.* Effects of particle irradiations on vortex states in iron-based superconductors. *Supercond. Sci. Tech.* **25,** 084008 (2012).
17. Maiorov, B. *et al.* Competition and cooperation of pinning by extrinsic point-like defects and intrinsic strong columnar defects in $BaFe_2As_2$ thin films. *Phys. Rev. B* **86,** 094513 (2012).
18. Haberkorn, N. *et al.* Influence of random point defects introduced by proton irradiation on critical current density and vortex dynamics of $Ba(Fe_{0.925}Co_{0.075})_2As_2$ single crystals. *Phys. Rev. B* **85,** 014522 (2012).
19. Lee, S. *et al.* Template engineering of Co-doped $BaFe_2As_2$ single-crystal thin films. *Nat. Mater.* **9,** 397–402 (2010).
20. Zhang, Y. *et al.* Self-assembled oxide nanopillars in epitaxial $BaFe_2As_2$ thin films for vortex pinning. *Appl. Phys. Lett.* **98,** 042509 (2011).
21. Maiorov, B. *et al.* Liquid vortex phase and strong c-axis pinning in low anisotropy $BaCo_xFe_{2-x}As_2$ pnictide films. *Supercond. Sci. Tech.* **24,** 055007 (2011).

22. Maiorov, B. *et al.* Angular and field properties of the critical current and melting line of Co-doped $SrFe_2As_2$ epitaxial films. *Supercond. Sci. Tech.* **22,** 125011 (2009).
23. Kasahara, S. *et al.* Evolution from non-Fermi- to Fermi-liquid transport via isovalent doping in $BaFe_2(As_{1-x}P_x)_2$ superconductors. *Phys. Rev. B* **81,** 184519 (2010).
24. Takeda, S. *et al.* Molecular beam epitaxy growth of superconducting $Sr_{1-x}K_xFe_2As_2$ and $Ba_{1-x}K_xFe_2As_2$. Appl. *Phys. Rev. B* **3,** 093101 (2010).
25. Holesinger, T. G. *et al.* Progress in nano-engineered microstructures for tunable high-current, high temperature superconducting wires. *Adv. Mater. Prog. Rep.* **20,** 391–407 (2008).
26. Blatter, G., Feilgl'man, M. V., Geshkenbein, V. B., Larkin, A. I. & Vinokur, V. M. Vortices in high-temperature superconductors. *Rev. Mod. Phys.* **66,** 1125–1388 (1994).
27. Mohan, S. *et al.* Transport and magnetic properties of Co-doped $BaFe_2As_2$ epitaxial thin films grown on MgO substrate. *Supercond. Sci. Tech.* **23,** 105016 (2010).
28. Baily, S. *et al.* Pseudoisotropic upper critical field in cobalt-doped $SrFe_2As_2$ epitaxial films. *Phys. Rev. Lett.* **102,** 117004 (2009).
29. Maiorov, B. & Civale, L. inFlux Pinning and AC Loss Studies on YBCO Coated Conductors. (eds Paranthaman, M. P. & Selvamanickam, V.) (Nova Science, 2007).
30. van der Beek, C. J. *et al.* Strong pinning in high-temperature superconducting films. *Phys. Rev. B* **66,** 024523 (2002).
31. Ijaduola, A. O. *et al.* Critical currents of *ex situ* $YBa_2Cu_3O_{7-\delta}$ thin films on rolling assisted biaxially textured substrates: thickness, field, and temperature dependencies. *Phys. Rev. B* **73,** 134502 (2006).
32. Solovyov, V. F. *et al.* High critical currents by isotropic magnetic-flux-pinning centres in a 3 micron-thick $YBa_2Cu_3O_7$ superconducting coated conductor. *Supercond. Sci. Tech.* **20,** L20–L23 (2007).
33. Miura, M. *et al.* Mixed pinning landscape in nanoparticle-introduced $YGdBa_2Cu_3O_y$ films grown by metal organic deposition. *Phys. Rev. B* **83,** 184519 (2011).
34. Lee, S. *et al.* Artificially engineered superlattices of pnictide superconductors. *Nat. Mater.* **12,** 392–396 (2013).
35. Cooley, L. D., Lee, P. J. & Larbalestier, D. C. Flux-pinning mechanism of proximity-coupled planar defects in conventional superconductors: evidence that magnetic pinning is the dominant pinning mechanism in niobium-titanium alloy. *Phys. Rev. B* **53,** 6638–6652 (1996).
36. Zhuang, C. G. *et al.* Significant improvements of the high-field properties of carbon-doped MgB_2 films by hot-filament-assisted hybrid physical-chemical vapor deposition using methane as the doping source. *Supercond. Sci. Technol.* **21,** 082002 (2008).
37. Godeke, A. A review of the properties of Nb_3Sn and their variation with A15 composition, morphology and strain state. *Supercond. Sci. Technol.* **19,** R68–R80 (2006).
38. Miura, M. *et al.* The effects of density and size of $BaMO_3$ (M = Zr, Nb, Sn) nanoparticles on the vortex glassy and liquid phase in $(Y,Gd)Ba_2Cu_3O_y$ coated conductors. *Supercond. Sci. Technol.* **26,** 035008 (2013).
39. Koshelev, A. E. & Kolton, A. B. Theory and simulations on strong pinning of vortex lines by nanoparticles. *Phys. Rev. B* **84,** 104528 (2011).

Acknowledgements

This work was supported by the Japan Society for the Promotion of Science, Japan, through the 'Funding Program for World-Leading Innovative R&D on Science and Technology Program'. M.M. is supported by the TEPCO Memorial Foundation, Japan. The work at Los Alamos National Laboratory was supported by the US DOE, Office of Basic Energy Sciences, Materials Sciences and Engineering Division (B.M.). We would like to thank Akira Takemori and Yasuo Oshikubo for photolithography preparation. M.M. would like to thank Jeffrey O. Willis for helpful discussions and critical reading of the manuscript.

Author contributions

M.M. grew the films, carried out experiment design, transport measurement and manuscript preparation. B.M. carried out data analysis, provided advice and consultation on flux pinning and prepared the manuscript. T.K. carried out microstructural studies. T.S. developed and processed the film and carried out XRD measurements. K.W. carried out transport measurements. S.A. worked on the laser system set-up. K.T. directed the research and contributed to manuscript preparations. All authors discussed the results and implications and commented on the manuscript.

Additional information

Competing financial interests: The authors declare no competing financial interests.

Reprints and permission information is available online at http://npg.nature.com/reprintsandpermissions/

How to cite this article: Miura M. *et al.* Strongly enhanced flux pinning in one-step deposition of $BaFe_2(As_{0.66}P_{0.33})_2$ superconductor films with uniformly dispersed $BaZrO_3$ nanoparticles. *Nat. Commun.* 4:2499 doi: 10.1038/ncomms3499 (2013).